Nanoscale

Accepted Manuscript

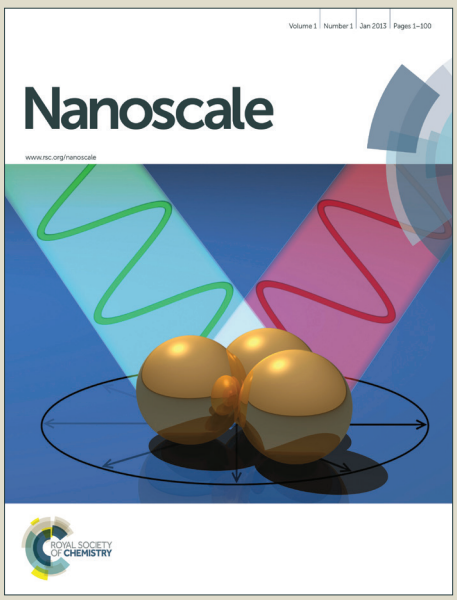

ROYAL SOCIETY OF CHEMISTRY

www.rsc.org/nanoscale

Journal Name

ARTICLE

Ex-situ electrochemical sodiation/desodiation observation of Co_3O_4 anchored carbon nanotubes: a high performance sodium-ion battery anode produced by a pulsed plasma in liquid

Received 00th January 20xx,
Accepted 00th January 20xx

DOI: 10.1039/x0xx00000x

www.rsc.org/

Md Mokhlesur Rahman,* Irin Sultana, Zhiqiang Chen, Mateti Srikanth, Lu Hua Li, Xiujuan J. Dai, Ying Chen

Liquid plasma, produced by nanosecond pulses, provides an efficient and simple way to fabricate a nanocomposite architecture of Co_3O_4/CNTs from carbon nanotubes (CNTs) and clusters of Co_3O_4 nanoparticles in deionized water. The crucial feature of the composite's structure is that Co_3O_4 nanoparticles clusters are uniformly dispersed and anchored with CNTs networks in which Co_3O_4 guarantees high electrochemical reactivity towards sodium and CNTs provides conductivity and stabilizes the anode structure. We demonstrate that Co_3O_4/CNTs nanocoposite is capable of delivering a stable and high capacity of 403 mA h g^{-1} at 50 mA g^{-1} after 100 cycles where the sodium uptake/extract is confirmed in the way of reversible conversion reaction by adopting *ex-situ* techniques. The rate capability of the composite is significantly improved and its reversible capacity is measured to be 212 mA h g^{-1} at 1.6 A g^{-1} and 190 mA h g^{-1} at 3.2 A g^{-1}, respectively. Due to the simple synthesis technique with high electrochemical performance, Co_3O_4/CNTs nanocomposites have a great potential as anode materials for sodium-ion batteries.

Introduction

Grid-scale electrical storage requires low cost, safe, and environmentally benign battery systems. Sodium-ion (Na-ion) batteries (SIBs) fulfil these requirements better than Li-ion batteries because Na is an earth abundant material.[1-3] However, widespread implementation of Na-ion batteries is significantly hindered by several major technological barriers, including low Na ion diffusion kinetics in electrodes, large volume changes, and structural pulverization during repeated charging/discharging, which are related to the larger size of Na^+ ions as compared to that of the Li^+ ions (1.02 vs 0.59 Å).[1, 4-7] As electrode materials are the key ingredients of any battery, therefore, the identification of materials suitable for effective use as anodes and cathodes of these devices is critical.

Most Na-ion battery research are focused on exploration of stable and low-cost cathode materials, [8] whereas less attention are paid to anode materials. Currently, there are increasing efforts on exploring the anode material, most of which are limited in nongraphitic carbonaceous materials. Hard carbon is the top ranked nongraphitic carbonaceous materials for sodium storage due to the large interlayer distance and the disorder structure,[2] but some disadvantages are revealed for non-graphitic carbonaceous materials such as the large irreversible capacity and poor capacity retention. It was found that anodes based on Na-alloying reaction can dramatically improve sodium storage capacity, however, large volume variation occurs with Na-alloy compounds during the charge/discharge process, which leads to rapid capacity loss. [9, 10]

Recently, as anodes for Na-ion batteries, many metal oxides with intercalation or conversion chemistries have been examined. Among them, most Ti-based oxides including TiO_2 (B), [11] $Na_2Ti_3O_7$, [12-15] $Na_2Ti_6O_{13}$, [16] $Na_4Ti_5O_{12}$, [17] $Li_4Ti_5O_{12}$, [18-20] and P2-$Na_{0.66}[Li_{0.22}Ti_{0.78}]O_2$, [21] store of Na^+ ions through intercalation chemistry and thus deliver relatively small reversible capacities of less than 300 mAh g^{-1} because of the limited number of storage sites in their crystalline structures. On the other hand, metal oxides which store Na^+ ions *via* a conversion reactions are of particular interest due to their high theoretical specific capacities of > 600 mAh g^{-1}. [22] Among metal oxides, transition metal oxides group are well known for lithium storage based on a conversion reaction mechanism, [23] but still seldom uninvestigated for analogous sodium storage. For example, Co_3O_4, follows a conversion reaction mechanism with lithium and has long been considered as one of the promising potential anode materials for Li-ion batteries due to its high theoretical capacity of 890 mAh g^{-1}. [24-27]

Regarding Na-ion batteries, a little attention has been paid to study electrochemical behaviors of Co_3O_4 with sodium. In 2014, we first attempted to extend the electrochemical investigation of cobalt oxide (Co_3O_4) with sodium and demonstrated a possible conversion reaction with a reversible capacity of 447 mA h g^{-1}. [28] Therefore, this work was undoubtedly helpful to further advance towards sodium electrochemistry of Co_3O_4 based electrodes. Later on, Wen et al. [29] also synthesized bowl-like hollow spherical Co_3O_4 structure and

Institute for Frontier Materials, Deakin University, Waurn Ponds, VIC 3216, Australia.
E-mail: m.rahman@deakin.edu.au

studied their sodium-storage behavior, however, electrochemical performance was unsatisfactory. It is widely accepted that the overall performance of Na-ion batteries is highly dependent on the inherent properties of the electrode materials. [2, 30] Metal oxides, especially transition metal oxides suffer from several problems when used as anode materials which limit their use, such as swelling and shrinking of active material particles upon the insertion and extraction of Li^+ or Na^+ ions, which induce poor contact due to pulverization between the active materials and the electron conducting agents, leading to low electric and ionic conductivity, [31] which directly affect their cycling stability and rate capability. Therefore, it is still a challenge to further improve sodium storage properties of Co_3O_4 based electrodes.

To solve these problems, one effective strategy is to fabricate composites of metal oxides with electronically conductive agents, such as carbon nanofibers, carbon nanotubes, and graphene, in which carbon materials act as a buffer matrix and a good electron transfer medium, and nanosized metal oxides particles alleviate the pulverization of the active material.[32-36] Moreover, the use of nanostructured metal oxide as electrode leads to improved electrochemical performances as it provides large surface area, numerous active sites, short mass and charge diffusion distance, and efficient accommodation of volume variation during repeated cycling process.[30, 31] Inspired by this strategy, Jian et al.[31] have developed Co_3O_4@CNTs composite where monodispersed hierarchical Co_3O_4 spheres intertwined with carbon nanotubes, which are capable to provide both facile electron and Na^+ ion diffusions in the system simultaneously. As a consequence, composite Co_3O_4@CNTs electrode exhibited improved cycling and rate performance. Recently, mesoporous Co_3O_4 sheets/3D graphene networks nanohybrids (Co_3O_4 MNSs/3DGNs) have been reported. [37] It is noticed that Co_3O_4 MNSs/3DGNs nanohybrids exhibit better SIBs performance with enhanced reversible capacity, good cycle performance and rate capability as compared to Co_3O_4 MNSs and Co_3O_4 nanoparticles, but rate capability was not as good as Co_3O_4@CNTs composite, which may be due to different conductive agents in both cases. It was found that Na-ion storage properties in carbon nanotubes (CNTs) is better than those of other carbon materials such as activated carbon, mesoporous carbon, and graphene nanosheets. [38]

In this work, we report a new "liquid plasma" method to fabricate Co_3O_4/CNTs nanocomposite using a nanosecond pulse atmospheric pressure plasma system (NPAPP) in a single step process. To the best of our knowledge, there is no report on the preparation of metal oxide based nanocomposite by adopting pulsed plasma in liquid. The sodium storage performance of the composite Co_3O_4/CNTs electrode is superior to that of the Co_3O_4 based electrode assembled *via* a conventional procedure. When used as a SIB anode, the nanocomposite exhibits a high reversible capacity of 403 mA h g^{-1} at 50 mA g^{-1} current after 100 cycles and shows a remarkable rate capability of 212 mA h g^{-1} at 1.6 A g^{-1} and 190 mA h g^{-1} at 3.2 A g^{-1}, respectively. Such a high rate capability is understood to be a consequence of incorporation of CNTs into Co_3O_4 clusters to form Co_3O_4/CNTs composite. In this composite, Co_3O_4 guarantees high electrochemical reactivity towards sodium, while the CNTs improves conductivity and stabilizes the anode structure. On the other hand, the electrochemical sodiation/desodiation process in Co_3O_4/CNTs system is determined by *ex-situ* X-ray diffraction (XRD) combined with high resolution TEM. Direct experimental evidence shows that Co_3O_4 undergoes reversible conversion reaction during cycling. This insight provides a significant advance for the understanding of electrochemical sodiation/desodiation process in transition metal oxide system.

Experimental

Synthesis of Co_3O_4 nanoparticles

The Co_3O_4 powder was synthesized by mixing together $CoCl_2 \cdot 6H_2O$ (Sigma-Aldrich, 98%), $LiNO_3$ (Sigma-Aldrich, 99.9%), $LiOH \cdot H_2O$ (Sigma-Aldrich, 98%), and H_2O_2 (Sigma-Aldrich, 35%) with a molar ratio of 0.01: 0.1: 0.02: 0.05, respectively, followed by grinding the mixture in a mortar with a pestle until it became homogenous. The mixture was immediately transferred to a muffle furnace and heat treated in air at 300°C for 3 h. At this temperature, the $LiNO_3$:$LiOH \cdot H_2O$:H_2O_2 mixture melted to become a molten salt solution. This is significantly different from an aqueous solution, and the water content in the molten salt solution was reduced as much as possible. After cooling naturally in air, the solid mass was washed with a large amount of DI water to dissolve unreacted salts and Co_3O_4 solid particles were separated by centrifugation. The product was then dried under vacuum at 100°C overnight to remove the residual water.

Preparation of Co_3O_4/CNTs nanocomposite

Liquid plasma was used to produce Co_3O_4/CNTs nanocomposite. Liquid plasma is a system that consists of a nanosecond pulse generator, two output channel electrodes, and the reaction chamber with 10 mL of DI water. [39] The two electrodes, with one electrode inside the liquid (bottom) and the other electrode 3 mm above the liquid (top). The molten salt synthesised Co_3O_4 powders and multi-walled carbon nanotubes (MCNTs) with a weight ratio of 10:1 were added to 10 mL of deionized water and magnetically stirred at a constant 1000 rpm for 5 min to make a uniform suspension. These uniformly suspended mixtures of Co_3O_4 and CNTs were then treated by the liquid plasma for 15 min with an argon gas flow rate of 0.083 L/min. The final product of Co_3O_4/CNTs was separated by centrifugation. The product was then dried under vacuum at 100°C overnight to remove the residual water. The schematic illustration of the composite preparation procedure is shown in Fig. 1.

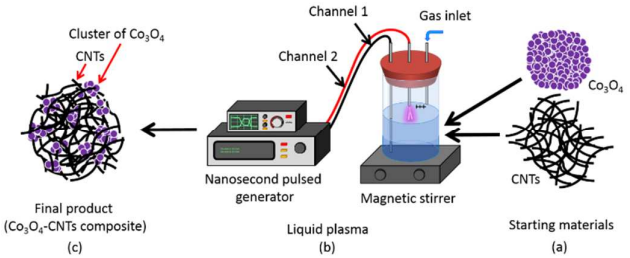

Fig. 1 Schematic view of composite preparation procedure: (a) starting ingredients of Co_3O_4 and CNTs; (b) nanosecond pulse atmospheric pressure plasma system using argon gas; and (c) final product of Co_3O_4/CNTs nanocomposite.

Material characterization

X-ray diffraction (XRD) data were collected from powder sample on a PANalytical X'Pert Pro instrument using a CuKa radiation source (λ = 1.54181 Å) and operated at 40 kV with 50 mA current. The X'Pert

data collector software in combination with the Joint Committee on Powder Diffraction Standards (JCPDS) powder diffraction files was used to identify the phases present. The morphology of each sample was examined using scanning electron microscopy (SEM, Carl Zeiss Supra 55 VP). Transmission electron microscopy (TEM) analysis was performed on a JEOL JEM 2100F instrument operated at 200 kV. Elastic image and energy-filtered elemental maps were acquired using a Gatan Quantum ER 965 Imaging Filter installed on the microscope, and a three-window method was used for acquiring elemental maps.

To test the electrochemical performance, Co_3O_4 and Co_3O_4/CNTs powder samples were mixed with acetylene carbon black (AB) and a binder, carboxymethyl cellulose (CMC), in a weight ratio of 80: 10: 10 in a solvent (distilled water), whereas CNT electrode was prepared by mixing only CNT powders and binder (CMC) with a weight ratio of 90:10, respectively. The slurry was spread onto Cu foil substrates and these coated electrodes were dried in a vacuum oven at 100^{o}C for 24 h. The average loading mass of active materials in the electrodes was ~1.4 mg. The electrode was then pressed using a disc with a diameter of 25 mm to enhance the contact between the Cu foil and active materials. Subsequently, the electrodes were cut to 1×1 cm^2. The electrochemical half cells were assembled in an Ar-filled glove box (Innovative Technology, USA) using CR 2032 coin cells with Na metal as the counter electrode, 1M $NaClO_4$ dissolved in propylene carbonate (PC) with 2 % FEC (fluoroethylene carbonate) additive as the electrolyte, and Whatman Glass Microfibre Filter (Grade GF/F) as a separator. The cells were galvanostatically discharged-charged in the range of 0.01-3.0V with a Land battery testing system. Cyclic voltammogram (CV) tests were performed on a Solartron Analytical electrochemical work station. For the *ex-situ* XRD measurements, the tested electrochemical cells were disassembled in an Ar-filled glove box. The cycled electrodes were taken out and washed with propylene carbonate (PC) to remove the residual electrolyte.

Results and discussion

XRD data were collected to study the crystal structure and purity of Co_3O_4 and composite Co_3O_4/CNTs samples (Fig. 2). Diffraction patterns indicate that both samples are consistent with the cubic phase of Co_3O_4 [JCPDS no. 00-043-1003, space group *Fd-3m* (no. 227)]. No peaks of any other phases or impurities were detected, demonstrating that materials with high purity could be obtain using the present synthesis strategy. The diffraction peaks at 19.0, 31.2, 36.8, 44.8, 59.3 and 65.21^o are associated with the 111, 220, 311, 400, 511, and 440 reflections of Co_3O_4, respectively, indicating successful synthesis of Co_3O_4.

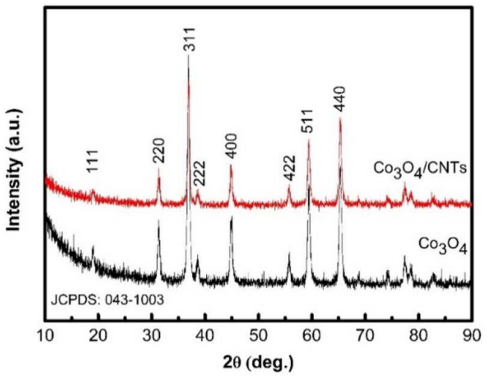

Fig. 2 X-ray diffraction patterns of Co_3O_4 and composite Co_3O_4/CNTs samples.

Fig. 3 shows SEM images of the samples. It is clearly seen that Co_3O_4 sample is composed of agglomerated clusters of nanoparticles (Fig. 3 (a)). A significant change in morphology is observed between Co_3O_4 and Co_3O_4/CNTs samples. For the Co_3O_4/CNTs composite sample, the SEM image (Fig. 3(b)) reveals that sample consists of numerous Co_3O_4 clusters and CNTs. It is very obvious that clusters are tightly wrapped in the CNTs networks. The homogeneous dispersion and intimate connectivity between Co_3O_4 clusters and CNTs can be expected to significantly increase conductivity and to stabilize the anode structure of the Co_3O_4/CNTs composite. A SEM image of CNTs is also depicted in Fig. 3 (c).

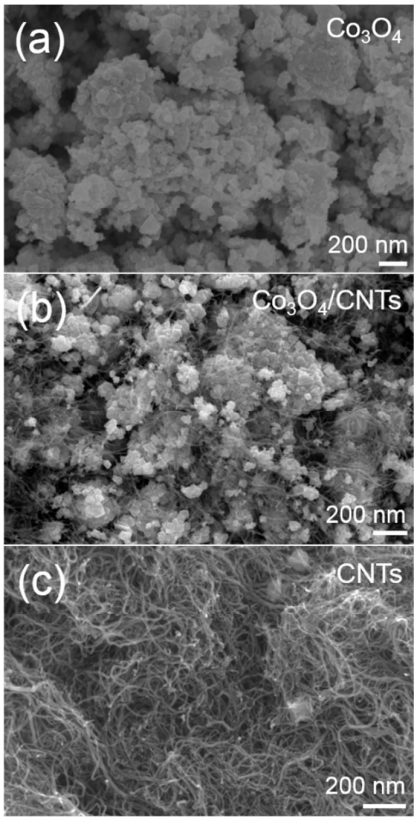

Fig. 3 SEM images of (a) Co_3O_4; (b) Co_3O_4/CNTs; and (d) CNTs samples.

The structure of each sample was visualised using TEM. Bright-field imaging of the Co_3O_4 sample reveals dense agglomerates of fine (< 20 nm) and much coarser (> 50 nm) crystalline Co_3O_4 (Fig. 4 (a)). The corresponding selected area electron diffraction (SAED) pattern is also depicted in Fig. 4 (b)). The SAED pattern consists of a single component of Co_3O_4 with *d* spacings of 0.476, 0.292, and 0.211 nm which can be referred to the crystallographic directions of (111), (220), and (400), respectively. These results are consistent with the XRD pattern obtained for this sample, as shown in Fig. 2. TEM observation of the composite Co_3O_4/CNTs sample is shown in Fig. 4 (c-e). It is found that the clusters of Co_3O_4 are not only anchored to the carbon nanotubes networks (Fig. 4 (c)), but also tightly wrapped

by the CNT networks (Fig. 4 (d)), ensuring that most of the particles can contribute to the charge/discharge process. The HRTEM image of the composite sample reveals lattice fringes of Co_3O_4 crystal (Fig. 4(e)).

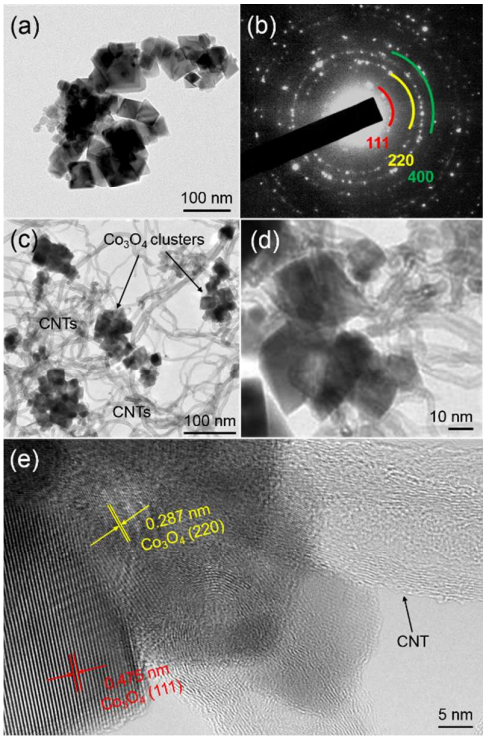

Fig. 4 TEM characterization: TEM images (a, b) of the Co_3O_4 sample: (a) a bright-field image and (b) SAED pattern of the sample; TEM images (c-e) of the composite Co_3O_4/CNTs sample: (c, d) bright-field images and (e) HRTEM image.

To obtain more detailed chemical information of the Co_3O_4/CNTs composite, additional TEM analysis was carried out. A bright-field STEM image and the corresponding energy-filtered elemental maps are shown in Fig. 5. The carbon map (Fig. 5(b)) and cobalt map (Fig. 5(c)) describe the location of CNTs networks and Co_3O_4 in the local area of Fig. 5(a), respectively. Fig. 5(d) depicts an overlay of carbon (CNTs) and cobalt (Co) maps, directly showing the distributions of CNTs (magenta colour) and Co_3O_4 (green colour) in the composite.

A series of comparative electrochemical measurements are performed to investigate the anode performance of Co_3O_4 and Co_3O_4/CNTs electrodes. Cyclic voltammograms (CV) of the electrodes are measured at a scan rate of 0.05 mV s^{-1} in the potential range of 0.01-3.0V (vs Na/Na^+) at room temperature (Fig. 6). In the CV curves, both electrodes exhibit a broad cathodic peak at ~ 0.4V and a shoulder peak at ~ 0.7V in the first cycle. This first cycle sodiation process corresponds to the reduction of Co_3O_4 to metallic cobalt (Co), the electrochemical formation of Na_2O, and the formation of an irreversible solid electrolyte interphase (SEI) layer. [28, 37] In the oxidation process (de-sodiation process), there is a peak at ~1.6 V for both electrodes, which corresponds to the re-oxidation of Co to Co_3O_4 and decomposition of Na_2O.

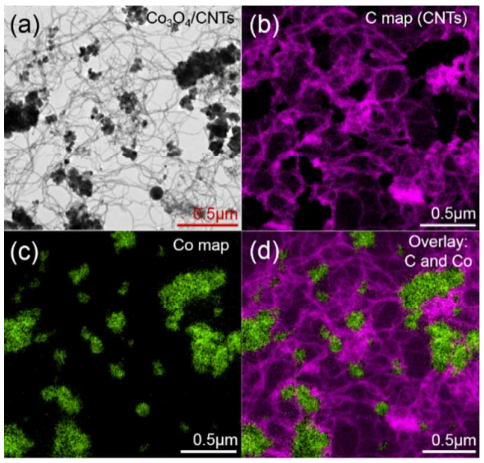

Fig. 5 Elemental maps of the Co_3O_4/CNTs composite: (a) a bright-field STEM image; (b, c) energy-filtered elemental maps of carbon (CNTs) and Co; and (d) an overlay of carbon and cobalt (colour scheme: carbon-magenta, cobalt-green).

The sodiation/de-sodiation process in the electrodes can be summarised by the following electrochemical reaction.

$$Co_3O_4 + 8Na^+ + 8e^- \leftrightarrow 4Na_2O + 3Co \quad (1)$$

From the second cycle, only one cathodic peak can be observed at ~ 0.55 and ~ 0.57 V for the Co_3O_4 and Co_3O_4/CNTs electrodes, respectively. The peaks intensity and the integral areas of all cycles (except first cycle) are very close to each other. These results show that the electrochemically reversibility of the electrodes is gradually improved after the first cycle. However, it is very hard to yield a strong redox peaks like that of lithium-ion batteries (LIBs) because of the large size, heavy mass, and poor mobility of Na^+. [28, 37, 40-42]

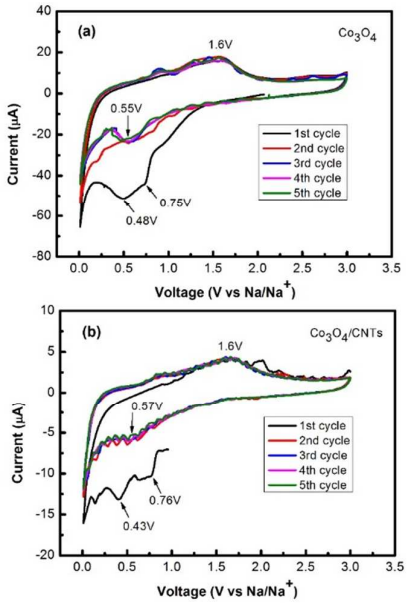

Fig. 6 Cyclic voltammogram of the (a) Co_3O_4 and (b) Co_3O_4/CNTs electrodes recorded at a scan rate of 0.05 mV s^{-1} between 0.01 and 3.0 V.

To evaluate the cycling performance of the electrodes, the galvanostatic charge and discharge measurements of the assembled cells are performed at a rate of 50 mAg^{-1} in the voltage range of 0.01-3V (vs Na/Na^{+}) at room temperature. Fig. 7 (a) shows the cycling stability of Co_3O_4, CNTs, and Co_3O_4/CNTs electrodes at a current density of 50 mA g^{-1}. It is clearly seen that composite Co_3O_4/CNTs electrode exhibits superior cycling performance, delivering the discharge capacity of 403 mAh g^{-1} after 100 cycles with a capacity retention of ~96% in respect to the 2nd cycle discharge capacity of 420 mAh g^{-1}. It is important to note that capacity contribution from CNTs (~20 mAh g^{-1}) is also considered because total weight of electrode active materials includes both Co_3O_4 and CNTs. In the case of pure Co_3O_4 electrode, a significant capacity fading is observed over the extended cycles. The discharge capacity is calculated to be approximately 208 mAh g^{-1} which represents only ~ 70% capacity retention. Compared with the Co_3O_4 electrode, the cycling performance (in terms of stability and discharge capacity) of Co_3O_4/CNTs electrode is much better, showing that the carbon nanotubes (CNTs) matrix have a positive effect to the system. Fig. 7 (b, c) shows the corresponding charge-discharge voltage profiles of the electrodes for the selected first, second, 50th, and 100th cycles. The first discharge curve displays all the characteristic features related to the various stages of sodiation. The first discharge profile exhibits a plateau around 0.8 V (SEI layer formation) followed by tail at a lower voltage, which confirms the existence of conversion process for the sodiation of Co_3O_4 and Co_3O_4/CNTs electrodes. However, the SEI layer formation voltage of the Co_3O_4 based electrode is different for Na-ion and Li-ion systems. [43, 44] In charging state, a significant plateau at ~1.6V is observed for both electrodes which is related to de-sodiation process due to decomposition of Na_2O. A commendable improvement of Coulombic efficiency of ~65% is measured in the first cycle for the Co_3O_4/CNTs electrode with respect to the Coulombic efficiency of Co_3O_4 (51%) electrode (Fig. 7 (d)). After initial few cycles, both electrodes exhibit high Coulombic efficiency of > 95%.

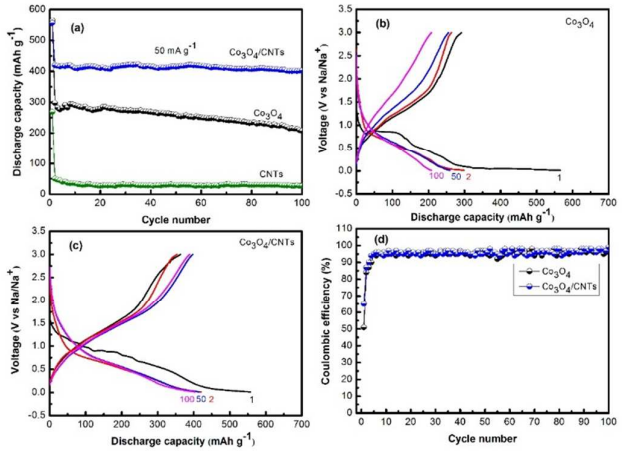

Fig. 7 Electrochemical performance of the electrodes in the voltage range of 0.01-3.0 V: (a) cycling stability up to 100 cycles at 50 mA g-1; (b, c) corresponding galvanostatic discharge-charge voltage profiles for the first, second, 50th, and 100th cycles; and (d) Coulombic efficiency up to 100 cycles.

Additional examination of the electrochemical performance of the Co_3O_4 and Co_3O_4/CNTs electrodes is shown in Fig. 8. The consecutive cycling behaviour at different charge-discharge rates, measured after 5 cycles in ascending steps from 0.05 to 3.2 A g^{-1}, followed by a return to 0.05 A g^{-1}, is presented in Fig. 8 (a). At the initial 5th cycle, the Co_3O_4/CNTs electrode shows a high discharge capacity of 410 mA h g^{-1} at 0.05 A g^{-1}, which is changed to 333 mA h g^{-1} at 0.1 A g^{-1}, 313 mA h g^{-1} at 0.3 A g^{-1}, 253 mA h g^{-1} at 0.8 A g^{-1}, 212 mA h g^{-1} at 1.6 A g^{-1}, and 190 mA h g^{-1} at 3.2 A g^{-1}. On the other hand, consecutive cycling performance of the pure Co_3O_4 electrode is unsatisfactory. After 35 cycles with different charge-discharge rates, the discharge capacity of the Co_3O_4/CNTs electrodes at 0.05 A g^{-1} is still 408 mA h g^{-1} which represents above 99 % capacity recovery. It can be seen that the Co_3O_4/CNTs electrode could tolerate a very high current rate and its reversible capacity is 212 mA h g^{-1} at 1.6 A g^{-1} and 190 mA h g^{-1} at 3.2 A g^{-1}, which is not only better than Co_3O_4 electrode but also much higher than that of the hard carbon anode materials currently used for Na-ion batteries. [45] The electrochemical impedance spectra of the Co_3O_4 and Co_3O_4/CNTs electrodes are shown in Fig. 8 (b). In the spectrum, the inclined lines in lower frequency region correspond to the Na diffusion process inside the electrode material and semicircle in the medium-frequency region is related to the charge-transfer resistance (R_{ct}) on electrolyte and the electrode interface. The Nyquist plots in the medium frequency range (100 kHz to 0.01 Hz) clearly show that the diameter of the semicircle of Co_3O_4/CNTs electrode is much smaller than that of the Co_3O_4 electrode, indicating that the Co_3O_4/CNTs electrode provides much easier charge transfer at the electrode-electrolyte interface and, consequently, decrease the overall cell's internal resistance. The incorporation of CNTs into Co_3O_4 by pulsed plasma in liquid medium significantly enhances the conductivity of the Co_3O_4/CNTs composite, since the CNTs provide conductive paths in the vicinity of the Co_3O_4 clusters, which is considered a key factor in improving the rate capability and cycling stability of the Co_3O_4/CNTs composite.

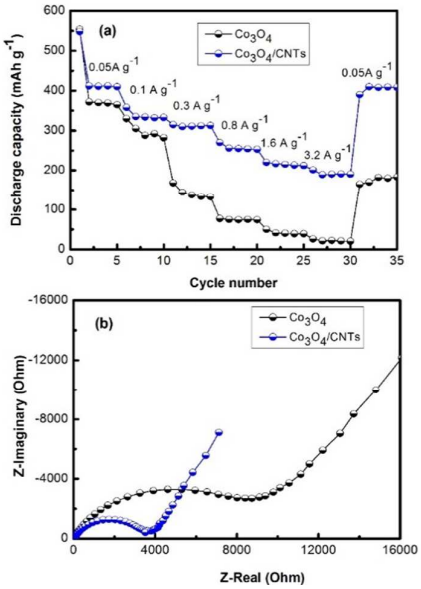

Fig. 8 Consecutive cycling performance and electrochemical impedance spectroscopy of Co_3O_4 and composite Co_3O_4/CNTs electrodes: (a) consecutive cycling performance at different current rates, ranging from 0.05 to 3.2 A g^{-1}, followed by a return to 0.05 A g^{-1}; and (b) electrochemical impedance spectroscopy of fresh cells (without cycling).

To realize the structural robustness and electrochemical sodiation/de-sodiation of the electrodes, a post-cycling investigations (Fig. 9) were carried out on the electrodes after 100 cycles at a current density of 50 mA g^{-1}. Fig. 9 (a, b) show the SEM and TEM images of the Co_3O_4 electrode and Fig. 9 (c-e) represent images of the Co_3O_4/CNTs electrode, respectively. It is obvious that the Co_3O_4 electrode develops large crack (Fig. 9 (a)) with particles aggregate (Fig. 9 (b)) which leads to active materials detachment from current collector, resulting in the deterioration in performance. In contrast, no obvious cracks are visible in the Co_3O_4/CNTs electrode (Fig. 9 (c)). However, the role of CNT as well as its distribution in the electrode are very difficult to understand from this SEM image. It seems that CNT is embedded in particles during cycling process. Therefore, additional TEM analysis was required for this purpose. Fortunately, morphology of the Co_3O_4/CNTs electrode sample remains well-preserved after sodiation/de-sodiation. Compared with the original morphology, clusters of Co_3O_4 nanoparticles still anchored with carbon nanotubes networks (Fig. 9 (d)), demonstrating that the CNTs matrix and Co_3O_4 nanoparticles can effectively accommodate the volume variation during cycling and alleviate the pulverization and aggregation of nanoparticles. The HRTEM image further demonstrates the distribution of CNTs and Co_3O_4 particles after cycling (Fig. 9 (e)).

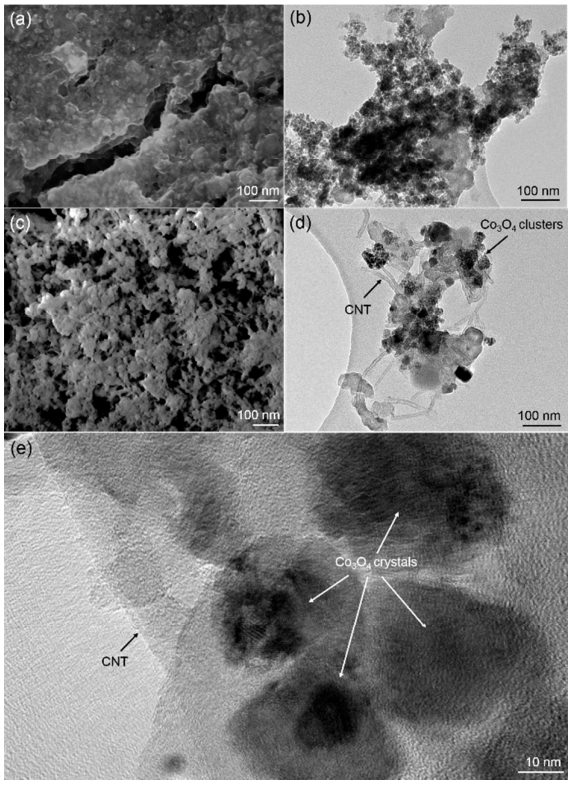

Fig. 9 Post-cycling investigations of the electrodes after 100 discharge-charge cycles at 50 mA g^{-1}: (a, b) images of Co_3O_4 electrode: (a) SEM image and (b) a bright-field TEM image; (c-e) images of Co_3O_4/CNTs electrode: (c) SEM image, (d) a bright-field TEM image, and (e) HRTEM image.

To determine the products after discharge-charge, *ex-situ* HRTEM and XRD were performed on electrodes after ten cycles. The SAED pattern of the Co_3O_4/CNTs electrode at discharging to 0.01V is shown in Fig. 10 (a). The SAED pattern shows the discharge products of Na_2O (200) and Co (111), respectively. When the electrode is charged back to 3.0 V, the SAED pattern (inset in Fig. 10 (b)) shows a single component of Co_3O_4 with a *d* spacing of 0.472, 0.290, 0.247, and 0.207 nm which are well matched with crystallographic directions of (111), (220), (311), and (400), respectively. The charge product of Co_3O_4 is also further confirmed by HRTEM analysis (Fig. 10 (b)) with a *d* spacing of 0.292 nm, which is in good agreement with (220) plane of Co_3O_4. To support the results obtained from *ex-situ* HRTEM investigation, the *ex-situ* XRD analysis of the fully discharged-charged electrodes for the 10th cycle is shown Fig. 10 (c). Being discharged to 0.01 V, there is an evidence of diffraction peak of Na_2O (JCPDS no. 00-003-1074). No Co peaks are observed. Unfortunately, there is significant overlap of these peaks with copper current collector peaks in the measured XRD patterns. When electrode was charged back to 3.0 V, all diffraction peaks for the Co_3O_4 phase reappeared. The above results clearly demonstrate that the electrochemical sodiation/de-sodiation of the Co_3O_4/CNTs electrode undergoes *via* reversible conversion reaction as described in equation (1).

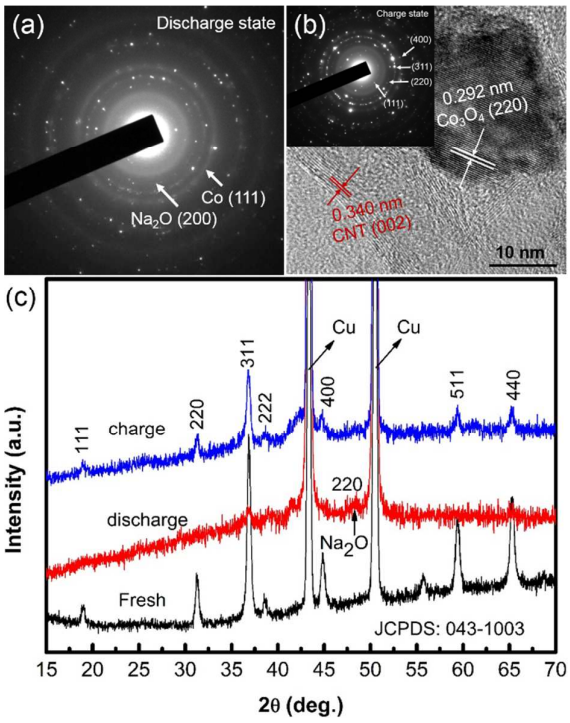

Fig. 10 *ex-situ* TEM and XRD on Co_3O_4/CNTs electrodes at 10th cycle: (a) SAED pattern at fully discharge state; (b) HRTEM image and inset

SAED pattern at fully charge state; and (c) XRD patterns at fully discharge and charge state.

The superior electrochemical performance of the Co_3O_4/CNTs electrode is attributed to the composite microstructure of the Co_3O_4/CNTs sample. In this composite structure, Co_3O_4 nanoparticles clusters anchored CNTs give a number of advantages such as (i) Co_3O_4 nanoparticles clusters significantly decrease the absolute stress/strain during the discharge-charge process; (ii) Co_3O_4 nanoparticles clusters anchored carbon nanotubes networks effectively accommodate the large volume change and prevent the aggregation of nanoparticles during Na-ion insertion and extraction processes; (iii) CNTs matrix provides electronic conductivity and stabilizes the anode structure; and (iv) both Co_3O_4 nanoparticles and carbon nanotubes (CNTs) reduce the traverse time for both electrons and sodium ions. These advantages result in a stable and increased reversible capacity as well as an improved rate capability. It is expected that this novel composite preparation technique can be extended to produce nanocomposites of other functional oxides.

Conclusions

A composite architecture of Co_3O_4/CNTs based on clusters of Co_3O_4 nanoparticles anchored carbon nanotubes (CNTs) has been prepared by combining a molten salt precipitation process and a liquid plasma for the first time. Microscopy investigation reveals that larger clusters of Co_3O_4 nanoparticles are reduced to smaller clusters under UV radiation in deionised water and uniformly dispersed along the chains of CNTs networks. Therefore, this novel composite structure plays a crucial role in the enhancement of electrochemical properties in sodium-ion batteries where both electron transfer and Na^+ ion diffusions take place simultaneously. The Co_3O_4/CNTs composite with a micro-nanostructure exhibits a stable cycling performance and superior rate capability. Hence, our smart electrode design enables Co_3O_4/CNTs composite to be a potential anode material for sodium-ion batteries.

Acknowledgements

Financial support from an Alfred Deakin Fellowship Award 2015 is acknowledged. Authors also acknowledge the support from Deakin Advanced Characterization Facility. The authors thank Dr Alexey M Glushenkov and Mr Debasis Poddar for their help with TEM.

Notes and references

1 S.W. Kim, D.H. Seo, X. Ma, G. Ceder and K. Kang, *Adv. Energy Mater.*, 2012, **2**, 710.
2 M.D. Slater, D. Kim, E. Lee and C.S. Johnson, *Adv. Funct. Mater.*, 2013, **23**, 947.
3 H. Pan, Y.S. Hu and L. Chen, *Energy Environ. Sci.*, 2013, **6**, 2338.
4 M. D. Slater, D. Kim, E. Lee and C. S. Johnson, *Adv. Funct. Mater.*, DOI: 10.1002/adfm.201200691.
5 A. Langrock, Y. Xu, Y. Liu, S. Ehrman, A. Manivannan and C. Wang, *J. Power Sources*, 2013, **223**, 62.
6 L. Fu, K. Tang, K. Song, P. A. Van Aken, Y. Yu and J. Maier, *Nanoscale*, 2014, **6**, 1384.
7 Y. Lu, N. Zhang, Q. Zhao, J. Liang and J. Chen, *Nanoscale*, DOI: 10.1039/c4nr06432a.
8 V. Palomares, P. Serras, I. Villaluenga, K. B. Hueso, J. C. Gonzalez and T. Rojo, *Energy Environ. Sci.*, 2012, **5**, 5884.
9 J. Qian, Y. Chen, L. Wu, Y. Cao, X. Ai and H. Yang, *Chem. Commun.*, 2012, **48**, 7070.
10 Y. Xu, Y. Zhu, Y. Liu and C. Wang, *Adv. Energy Mater.*, 2013, **3**, 128.
11 J. P. Huang, D. D. Yuan, H. Z. Zhang, Y. L. Cao, G. R. Li, H. X. Yang and X. P. Gao, RSC Adv., 2013, **3**, 12593.
12 A. Rudola, K. Saravanan, C. W. Mason and P. Balaya, *J. Mater. Chem. A*, 2013, **1**, 2653.
13 P. Senguttuvan, G. Rousse, V. Seznec, J. M. Tarascon and M. R. Palacin, *Chem. Mater.*, 2011, **23**, 4109.
14 W. Wang, C. Yu, Z. Lin, J. Hou, H. Zhu and S. Jiao, *Nanoscale*, 2013, **5**, 594.
15 W. Wang, C. Yu, Y. Liu, J. Hou, H. Zhu and S. Jiao, *RSC Adv.*, 2013, **3**, 1041.
16 A. Rudola, K. Saravanan, S. Devaraj, H. Gong and P. Balaya, *Chem. Commun.*, 2013, **49**, 7451.
17 S. H. Woo, Y. Park, W. Y. Choi, N.-S. Choi, S. Nam, B. Park and K. T. Lee, *J. Electrochem. Soc.*, 2012, **159**, A2016.
18 X. Yu, H. Pan, W. Wan, C. Ma, J. Bai, Q. Meng, S. N. Ehrlich, Y.S. Hu and X.Q. Yang, *Nano Lett.*, 2013, **13**, 4721.
19 Y. Sun, L. Zhao, H. Pan, X. Lu, L. Gu, Y.-S. Hu, H. Li, M. Armand, Y. Ikuhara, L. Chen and X. Huang, *Nat. Commun.*, 2013, **4**, 1870.
20 L. Zhao, H. L. Pan, Y. S. Hu, H. Li and L. Q. Chen, *Chin. Phys.*, 2012, **21**, 028201.
21 Y. Wang, X. Yu, S. Xu, J. Bai, R. Xiao, Y.S. Hu, H. Li, X.Q. Yang, L. Chen and X. Huang, *Nat. Commun.*, 2013, **4**, 2365.
22 Y. Kim, K. H. Ha, S. M. Oh and K. T. Lee, *Chem. Eur. J.*, 2014, **20**, 11980.
23 P. Poizot, S. Laruelle, S. Grugeon, L. Dupont and J.M. Tarascon, *Nature*, 2000, **407**, 496.
24 L. Li, K. H. Seng, Z. Chen, Z. Guo and H. K. Liu, *Nanoscale*, 2013, **5**,1922.
25 N. Du, H. Zhang, B. D. Chen, J. B. Wu, X. Y. Ma, Z. H. Liu, Y. Q. Zhang, D. R. Yang, X. H. Huang and J. P. Tu, *Adv. Mater.*, 2007, **19**, 4505.
26 J. S. Chen, T. Zhu, Q. H. Hu, J. Gao, F. Su, S. Z. Qiao and X. W. Lou, *ACS Applied Materials & Interfaces*, 2010, **2**, 3628.
27 X. W. Lou, D. Deng, J. Y. Lee and L. A. Archer, *J. Mater. Chem.*, 2008, **18**, 4397.
28 M. M. Rahman, A. M. Glushenkov, T. Ramireddy and Y. Chen, *Chem. Commun.*, 2014, **50**, 5057.
29 J.W. Wen, D.W. Zhang, Y. Zang, X. Sun, B. Chen, C.X. Ding, Y. Yu and C.H. Chen, *Electrochim. Acta*, 2014, **132**, 193.
30 V. Palomares, M. C. Cabanas, E. C. Martínez, M.H. Hanb and T. Rojo, *Energy Environ. Sci.*, 2013, **6**, 2312.
31 Z. Jian, P. Liu, F. Li, M. Chen and H. Zhou, *J. Mater. Chem. A*, 2014, **2**, 13805.
32 L. Wu, X.H. Hu, J.F. Qian, F. Pei, F.Y. Wu, R.J. Mao, X.P. Ai, H.X. Yang and Y.L. Cao, *Energy Environ. Sci.*, 2014, **7**, 323.
33 D.Y.W. Yu, P.V. Prikhodchenko, C.W. Mason, S.K. Batabyal, J. Gun, S. Sladkevich, A.G. Medvedev and O. Lev, *Nat. Commun.*, 2013, **4**, 2922.
34 Y.J. Zhu, X.G. Han, Y.H. Xu, Y.H. Liu, S.Y. Zheng, K. Xu, L.B. Hu and C.S. Wang, *ACS Nano*, 2013, **7**, 6378.
35 D.W. Su, H.J. Ahn and G.X. Wang, *Chem. Commun.*, 2013, **49**, 3131.
36 M.H. Liang and L.J. Zhi, *J. Mater. Chem.*, 2009, **19**, 5871.
37 Y. Liu, Z. Cheng, H. Sun, H. Arandiyan, J. Li and M. Ahmad, *J. Power Sources*, 2015, **273**, 878.
38 Y. Wang, D. Su, C. Wang and G. Wang, *Electrochem. Commu.*, 2013, **29**, 8.
39 S. B. Ponraj, Z. Chen, L. H. Li, J. S. Shankaranarayanan, G. D. Rajmohan, J. Plessis, A. J. Sinclair, Y. Chen, X. Wang, J. R. Kanwar and X. J. Dai., *Langmuir*, 2014, **30** (35), 10712.
40 M. M. Rahman, J. Z. Wang, X. L. Deng, Y. Li and H. K. Liu, *Electrochim. Acta*, 2009, **55**, 504.
41 J. Chen , L. N. Xu , W. Y. Li and X. L. Gou, *Adv. Mater.*, 2005, **17**, 582.
42 M. Valvo, F. Lindgren, U. Lafont, F. Björefors and K. Edström, *J. Power Sources*, 2014, **245**, 967.
43 X. Guo, W. Xu, S. Li, Y. Liu, M. Li, X. Qu, C. Mao, X. Cui and C. Chen, *Nanotechnology*, 2012, **23**, 465401.

44 X. Yang, K. Fan, Y. Zhu, J. Shen, X. Jiang, P. Zhao and C. Li, *J. Mater. Chem*., 2012, **22**, 17278.
45 K. Tang, L. Fu, R. J. White, L. Yu, M. M. Titirici and M. Antonietti, J. Maier, *Adv. Energy Mater.*, 2012, **2**, 873.